Available online at www.sciencedirect.com

ScienceDirect

materialstoday: PROCEEDINGS

Materials Today: Proceedings 3 (2016) 294 – 302

Advances in Functional Materials (Conference 2015), AFM 2015

An advance towards the synthesis of Ag nanorod arrays with controlled surface roughness for SERS substrates

M. Gómez-Gómez[a]*, J. Calderón[a], R. Abargues[b], P. J. Rodríguez-Cantó[b], I. Suárez[a], J. P. Martínez Pastor[a], D. Hill[a]

[a]*Instituto de Ciencias de los Materiales, Universidad de Valencia, PO Box 22085, 46071 Valencia, Spain*
[b]*Intenanomat S. L., Catedrático José Beltrán 2, 46980 Paterna, Spain*

Abstract

An innovative approach to produce silver nanorod (NRs) arrays with controlled morphological parameters and surface roughness is presented. The Ag NRs were obtained using a three-stage fabrication process based on the electron beam exposure of a metal-polymer nanocomposite resist on a transparent substrate and development, a post bake and then a series of non-electrochemical metallization steps. After each step the evolution of the Ag NRs was characterized by scanning electron microscopy (SEM) for morphology and optical transmittance (T) measurements for Localized Surface Plasmon Resonance (LSPR). The transmittance measurements were interpreted using models based on the Finite Element Method (FEM).

Selection and peer-review under responsibility of Conference Committee Members of Advances in Functional Materials (Conference 2015).

Keywords: Plasmon; nanocomposite; COMSOL; SERS; LSPR; Nanorod.

* Corresponding author. Tel.: +34 651399084; fax: +34 963543633.
E-mail address: maria.i.gomez@uv.es

Selection and peer-review under responsibility of Conference Committee Members of Advances in Functional Materials (Conference 2015).
doi:10.1016/j.matpr.2016.01.072

1. Introduction

When metal nanoparticles are excited by light of a specific wavelength, their conduction electrons exhibit collective oscillations known as localized surface plasmon resonance (LSPR) [1]. The collective oscillations of the electrons enhance the electromagnetic field significantly at the surface of the nanostructure. The LSPR of the nanoparticles is highly dependent on their geometry, metal composition, and the dielectric function of their surrounding medium. The ability to tune the LSPR of metal nanoparticle systems is desirable for many technological applications. The fabrication of metallic nanostructures on transparent substrates with high electric field enhancement factors remains the focus of much research due to their potential integration into Lab on Chip devices, on their own, or as part of multiparametric sensing [2-5]. The enhancement of the electric field on the surface of metallic nanostructures greatly enhances the Raman scattering, one of the principal mechanisms contributing to Surface Enhanced Raman Scattering (SERS). Nanoscale surface roughness in metal nanoparticles can give rise to significantly higher local field enhancement compared to those obtained with smooth particles [6, 7]. In this paper we report the use of a synthesis method to obtain on transparent substrates Ag nanorods (NRs) with controllable surface roughness and other characteristic morphological parameters (width, length, horizontal and vertical separation) in an array format on transparent substrates.

2. Samples

2.1. Description of the design

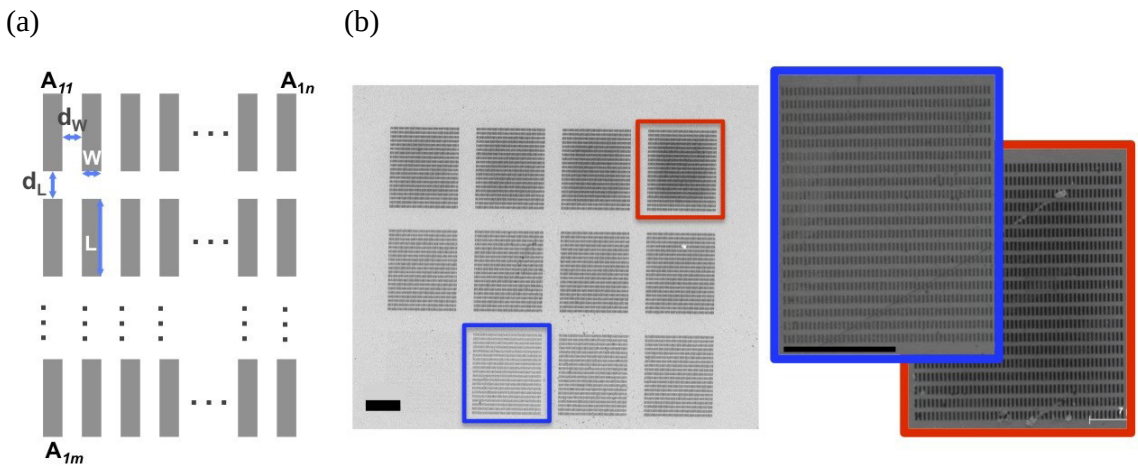

Fig. 1 (a) Design schematic of the Ag NRs arrays. (b) A SEM image of the arrays after the first (i) fabrication stage, scale bar: 10 µm. Twelve different electron doses were tested, the lowest one employed when processing the array located at lower left-hand corner of the picture, increasing from left to right, and from bottom to top of the image. The two insets, blue and red edged, are enlarged SEM micrographs of the array obtained under the second lowest and the highest electron flux, respectively, scale bar:10 µm.. All images were taken under the same conditions, the differences in contrast being due the quantity of NPs formed in this step.

A synthesis method based on metal-polymer resist nanocomposite was used to obtain Ag nanorods (NRs) on transparent substrates in array format with controllable morphological parameters. The design parameters include the width, W=100 nm and length, L=400 nm of the NRs, the distance between each two consecutive Ag NRs, widthways, d_w=100, and longways, d_L=200, respectively, and an array (A) size *mxn* of 30x80, as depicted in Fig. 1 (a).

2.2. Fabrication

The fabrication process for the Ag NRs consists of applying a three-stage procedure to a metal-polymer nanocomposite resist on a transparent SiO_2-ITO substrate. The three stages are: (i) exposure of a nanorod array design pattern by electron beam lithography (EBL) followed by development, (ii) an in-situ synthesis of metal NPs during the post-bake, (iii) non electrochemical metallization of the nanocomposite nanorods in multiple steps [8,9]. These steps consisted of immersing the sample into a solution of the corresponding precursor metal salt and a suitable reducing agent giving rise to the growth of the Ag NPs, and subsequent pattern metallization [9].

As a means to optimize the first stage (i), and thereby control the characteristic morphological parameters of the resulting nano-patterns, twelve different electron doses were used, one for each array, an overview of the resulting arrays is shown in Fig. 1(b). As expected, for higher electron doses more NPs were generated at this first stage of the process, being the seeds for the next stage, as seen in Fig. 1(b).

3. Characterization

Characterization mainly focused on the effects of metallisation steps of different durations in stage (iii) of the fabrication process, specifically the evolution of the NPs within the NRs. The effect of different metallisation durations, or regrowth times, labelled as RG1, RG2, etc., on the morphological and optical properties of the NRs was monitored by scanning electron microscopy (SEM) and optical transmittance (T) measurements. For RG1 to RG3 no noticeable changes in the morphology and optical transmittance were detected and so here we report instead just the significant changes observed over RG4 and RG5.

3.1. Morphological study of the growth process

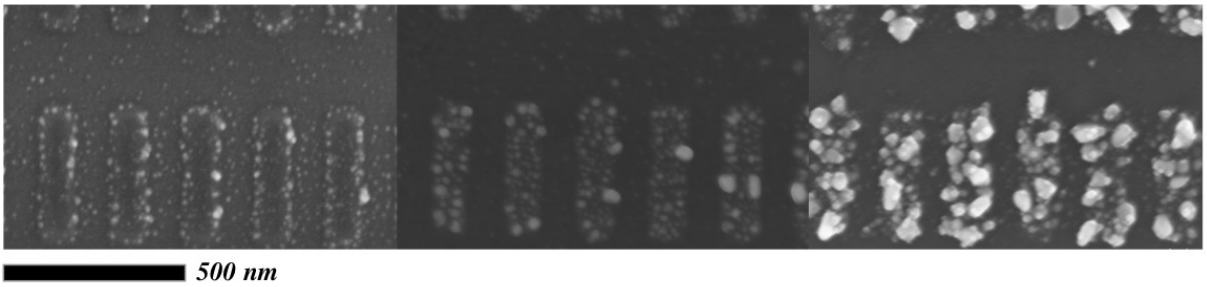

Fig. 2 SEM micrograph of the sample after stage (ii) of the fabrication process (a) and subsequent RG4 (b) and RG5 (c) iterations of stage (iii)

Following stages (i) and (ii) embedded Ag NPs, which act as seeds for the subsequent metallisation steps, can be seen to have approximate diameters of 10 nm within the polymer matrix (Fig. 2 (a)) whilst following RG4 (Fig. 2b) those diameters have spread to within 10-25 nm. After another iteration, RG5, a noticeable increase in the size of Ag NPs is observed as expected, and so surface roughness, with a number of Ag NPs with diameter values ~65 nm being observed. Moreover, the separation of particles has reduced with some even overlapping. In terms of characteristic morphological parameters (W, L, d_w and d_L) and the deviation of their measured values from nominal or design ones, differences were unnoticeable immediately after RG4 whilst following RG5, measured d_w became 15 nm smaller and W~10 nm larger. For L and d_L no relevant deviations were ever observed.

3.2. Optical characterization of the growth process

At a wavelength equal to the excitation of a LSPR a minima occurs within the T spectra of plasmonic structures. Therefore, in order to characterize the plasmonic properties of the sample with the gradual metallization of the NRs,

T was measured for the Ag NRs arrays both perpendicular and parallel to their major axis after each RG iteration in stage (iii). Following RG4 a broad band minimum extending between 525 nm and 825 nm, with its peak centred at ~700 nm, is seen for both polarisations (Fig. 3(b)), whilst immediately after RG5 spectrum changes dramatically with the minimum blue shifting to ~520 nm and becoming significantly more pronounced, for both polarizations.

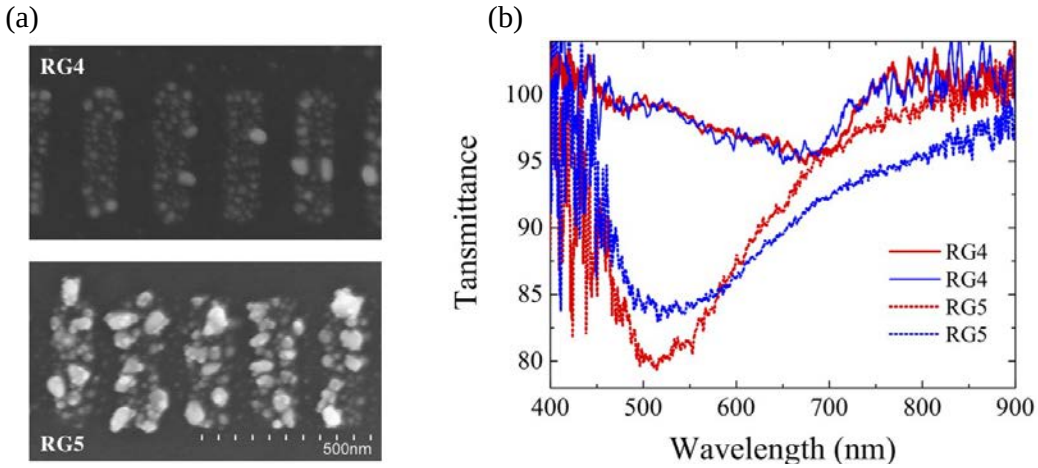

Fig. 3 (a) SEM images of nanocomposite NR structures following RG4 and RG5 respectively. (b) Transmittance spectra measured both perpendicular (red) parallel (blue) to the major axis or the rods following RG4 and RG5, indicated as continuous and dashed lines, respectively.

4. Numerical study of the localized surface plasmon resonance (LSPR) and electric field distribution

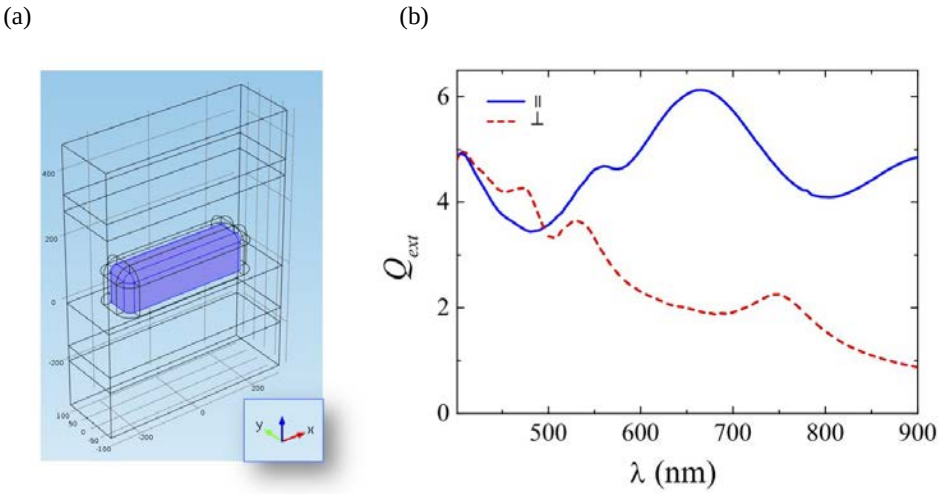

Fig. 4 (a) Schematic of simulated Ag NR, where L= 400 nm, W=100 nm, Curvature radius at edges = 20 nm, d_1=100, d_2=200, h=120 nm. (b) Extinction efficiencies obtained from the numerical simulation under parallel and perpendicular polarization.

In order to analyse and interpret more accurately the transmission data (T), the LSPR of the NR's arrays with same characteristic morphological parameters as those fabricated were modelled. In a first approach, Ag NRs with smooth surfaces, as shown in **Fig. 4** (a) were assumed. The model was simulated using COMSOL [10], a commercial software

based on the finite element method (FEM), following previous LSPR modelling of other metallic nanostructures [11-13]. In the model, two semi-infinite media (air and SiO_2) are present. The real and imaginary refractive indices of silver are modelled through an interpolation with splines of the experimental data obtained by Rakić et al. [14]. Thereafter a linearly polarized electromagnetic plane wave is sent from the surrounding media under normal incidence. A sweep through different wavelengths for both polarizations is then performed in order to obtain the characteristic plasmonic spectra.

The wavelength dependence of the extinction coefficient, Q_{ext}, is depicted in **Fig. 4**(b), with the spectrum for each polarization demonstrating significantly different features. For E polarized perpendicular to the major axis of the NRs, three peaks can be seen in the visible (VIS) region of the spectrum: the primary plasmon peak at 405 nm together with two subsequent peaks, at 475 nm and 535 nm, diminishing in intensity from shorter to longer wavelengths. In the IR region a broader and less intense peak at ~750 nm appears. When E is polarised parallel to their major axis, in contrary to the perpendicular polarization, the primary plasmon resonance is located at longer wavelengths, in the near infrared (NIR) region, with a broad band ranging from 580 to 780 nm, with the peak centred at 665 nm. At lower wavelengths a peak centred at 555 nm appear overlapped to the primary peak. At higher wavelengths a broad peak centred about 920 nm was also predicted.

In general this polarization dependence of Q_{ext} did not manifest itself in the T experimental data (**Fig. 3** (b)), possibly because the NRs are constituted actually by Ag NPs randomly located, this fact changes the symmetry conditions and is not possible to distinguish the expected inherent built-in plasmonic effects due to the anisotropy of the NRs. Only for the parallel configuration Q_{ext} is in good agreement with the T minimum band observed following RG4, suggesting that it is due to the longitudinal plasmon on the NRs. The characteristic minimum measured after RG5 could be assigned to the transversal plasmon, since after the RG5 the NPs have significantly grown diminishing the d_W and satisfying the condition $d_W/W<W$. However, as the surfaces of the experimental NRs are not perfectly smooth that minimum could be also ascribed to the LSPR of Ag NPs on the surface of the NRs. After RG5 the number of NPs with diameter (D) ~ 65 increases with LSPR expected to be ~ 500 nm, moreover, the nanoparticle separation distance becomes smaller leading to redshift of the plasmon resonance. The combination of both of these effects for the Ag NPs on the surface of the NRs could explain the blue shift to ~520 nm of the experimental T minimum following RG5.

The electric field enhancement factor for surface enhanced Raman scattering (SERS) arising from such nanostructures with smooth surfaces was also numerically modelled (**Fig. 5**) in order to determine the dependence of the SERS signal with the surrounding volume of the NRs comprised from their surfaces to 20 nm above, since this is the distance that generally dramatically diminishes the SERS effect. When the electric field is along the parallel direction a broadband centred ~700 nm appears, and so an enhancement of the Raman signal would be expected when exciting in this configuration with laser wavelengths close to ~700 nm. If the polarization is perpendicular the dominant feature would be a peak in the VIS region, close to 500 nm.

Finally, electric field profiles at the LSPR frequency in the NIR region (750 nm) were modelled both for smooth and rough Ag. **Fig. 6** (a) and (c) show the E field distribution when E is parallel to the major axis of the Ag NR, enhanced E fields occur around the corners of the NR, from just below the rounded edges to just on the top surface of the Ag NR. **Fig. 6** (b) and (d) display the E field distribution when E is perpendicular, in this case the E fields occur not only at the corners of the NRs, but also at the edges along the longer axis of the NR, reaching higher concentrations at the centre of their length, with greater fields at z=h than in z=h-R/2. These E fields are due to transversal mode electron oscillations in the nanorod. On both sections, z=h and z=h-R/2 it is observed that when E field polarization is along the perpendicular direction, there is higher field density in the middle of the surfaces along the major axis, evidencing the E field coupling effects between near neighbours along the perpendicular direction.

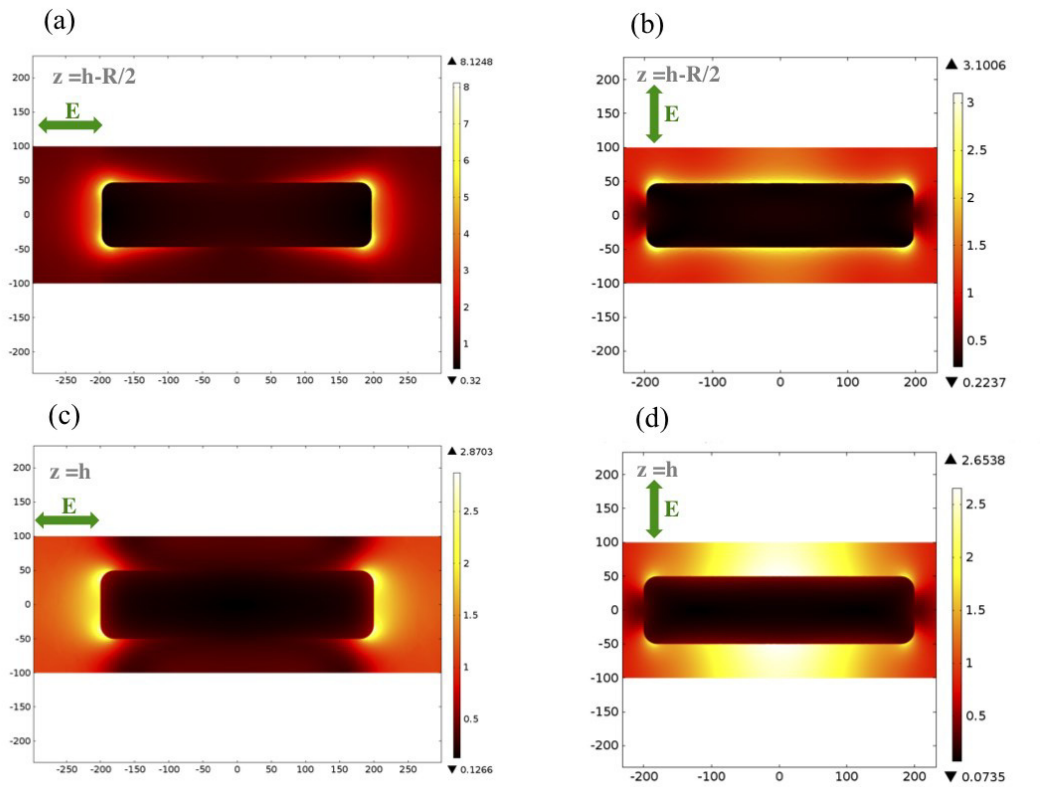

Fig. 5 Normalized SERS enhancement factor, in volume, (G^V) as function of wavelength for E polarized parallel and perpendicular to the major axis of the NRs

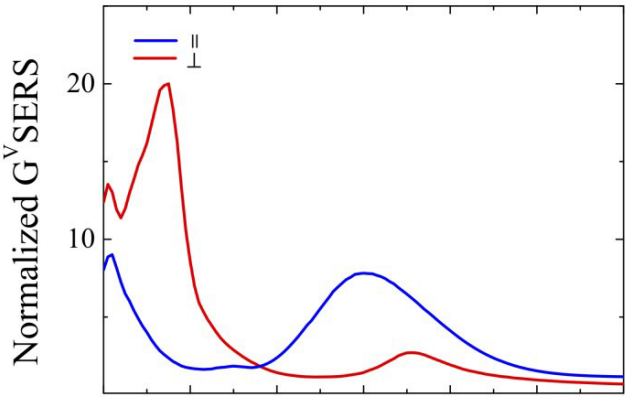

Fig. 6 xy electric field distribution of a smooth NR with characteristics parameters: L= 400 nm, W=100 nm h= 120 nm and the radius of the rounded corners r= 20 nm, at different z of the NR. (a) z= h-r/2 and (c) z=h, assuming parallel polarization. (b) z=h-r/2 and z=h, assuming perpendicular polarization.

For the simulation the roughness of the NRs due to the Ag NPs that constitute them was taken into account based on the geometric design depicted in **Fig. 7**. The NR consists on a matrix of PVA (refractive index *n*=1.52), the hosting material, with the same geometrical parameters as the Ag NRs with smooth surfaces showed below, containing a 3D array of Ag nanospheres (NSs) of diameters ~20 nm and interparticle distance of 10 nm (30 nm from centre to centre of the NSs) [15]. For the uppermost layer of this 3D distribution, a set of larger NSs (with diameters=40 to 60 nm) with random inter-particle distances and positions was added so as to replicate the surface appearance of the fabricated NRs.

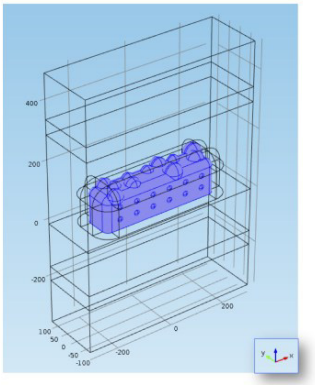

Fig. 7 Schematic of the NR with the embedded Ag NPs

In contrary to that of the smooth NRs, in this case E field distribution due to the NR as a dipole is suppressed independently of the E field polarization and planar section, demonstrating the effect of the internal discontinuities. For the section, z=h (**Fig. 8** (c) and (d)), the effect of polarization on the hot spot locations can be seen, although, as expected they are restricted shortest distances between NPs. Furthermore, the same section shows an important enhancement of the E field density, for potential applications for SERS measurements.

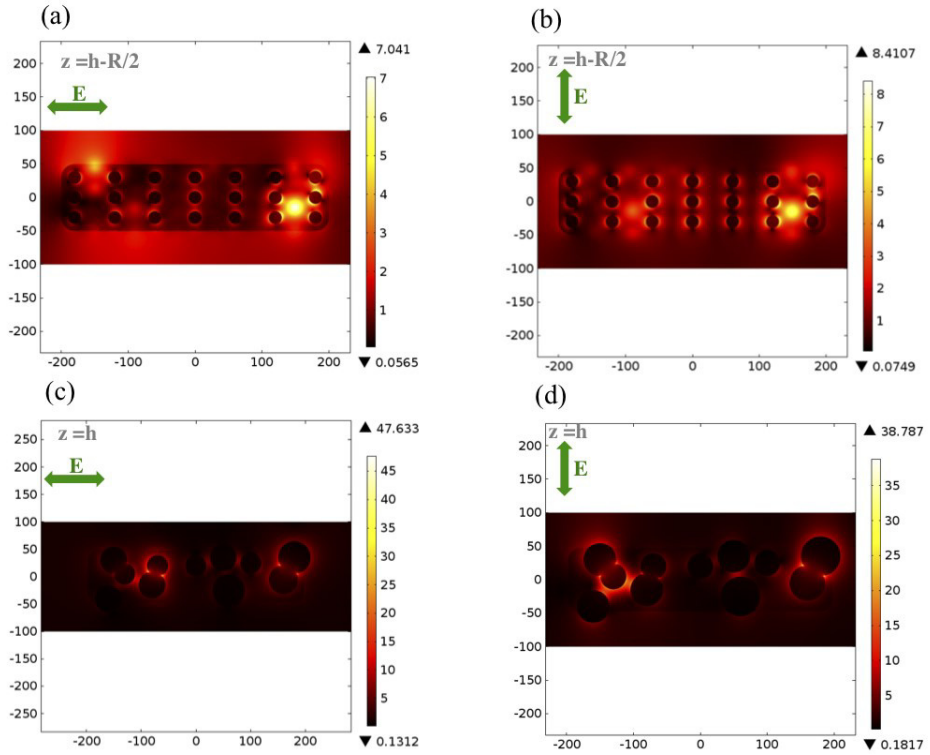

Fig. 8 xy electric field distribution of a NR taking into account the NPs (a) z= h-r/2 and (c) z=h, assuming parallel polarization. (b) z=h-r/2 and (d) z=h, assuming perpendicular polarization.

5. Conclusions

The reproducibility of Ag NRs fabricated with geometrical dimensions down 500 nm has been demonstrated for a synthesis based fabrication method, as has a controlled slow increase in the diameter of the constituting NPs through iterative metallisation steps. The fabrication method therefore allows a good control of the characteristics morphological parameters of including their surface roughness. Numerical simulations have been carried out in order to discriminate the origin of the unexpected features of the optical transmittance spectrum after RG5, and to compare the E field distribution for rough and smooth Ag NRs. The NRs with rough surfaces demonstrated an important enhancement of the E field density that could be exploited for SERS measurements. We aim to do further modelling the Q_{ext} for the rough surfaces in order to shed more light into the optical properties tested experimentally.

Acknowledgements

This work was carried out within the FP7-ICT-610472-CanDo project, funded by the European Commission.

References

[1] K. A. Willets, R. P. Van Duyne Van der Geer, Localized Surface Plasmon Resonance Spectroscopy and Sensing, Annu. Rev. Phys. Chem. 58 (2007) 267–97.
[2] Y. Hong, Y-M. Huh, D. Sung Yoon, Nanobiosensors Based on Localized Surface Plasmon Resonance for Biomarker Detection, J. of Nanomaterials, 2012 (2012) 759830
[3] S. Michaelis, J. Wegener, R. Robelek, Label-free monitoring of cell-based assays: Combining impedance analysis with SPR for multiparametric cell profiling. Biosensors & Bioelectronics 39 (2013) 63-70
[4] H. Hsien Wang, T. You Cheng, T. Sharma, Ch. Fang-Yi, S. W. Yu Chiu, J. Kai Wang, Y. Lin Wang, Transparent Raman-enhacing substrates for microbiological monitoring and in situ pollutant detection. Nanotechnology 38 (2011) 38570.
[5] L. Rodríguez-Lorenzo, L. Fabris, R. A. Álvarez-Puebla, Multiplex optical sensing with surface-enhanced Raman scattering: A critical review, 745 (2012) 10-23.
[6] J. Rodríguez-Fernández, A. M. Funston, J. Pérez-Juste, R. A. Álvarez-Puebla, L. M. Liz-Marzán P. Mulvaney, Phys. Chem. Chem. Phys, 11 (2009) 59059-5914
[7] W. A. Murray, W. L. Barnes, Plasmonic Materials, Advanced Materials, 19 (2007)3771-3782.
[8] R. Abargues, J. Marqués-Hueso, J. Canet-Ferrer, E. Pedrueza, J. L. Valdés, E. Jiménez, J. P. Martínez-Pastor, High-Resolution Electron-Beam Patternable Nanocomposite Containing Metal Nanoparticles For Plasmonics. Nanotechnology, 19, (2008) 355308.
[9] R. Abargues, M. L. Martínez-Marco, P. J. Rodríguez-Canto, J. Marqués-Hueso, J. P. Martínez-Pastor, Metal-Polymer Nanocomposite Resist: A Step Towards In-Situ Nanopatterns Metallization. Proc. Spie (2013) 8682.
[10] COMSOL Multiphysics, Comsol Inc. (http://www.comsol.com)
[11] J. Calderón, J. Álvarez, P. J. Martínez-Pastor, D. Hill, Modelling Of Polarimetric Lspr Sensing With Bowtie Nanoantennas Arrays. Europtrode Xii (2014)
[12] J. Calderón, J. Álvarez, P. J. Martínez-Pastor, D. Hill, Bowtie Plasmonic Nanoantenna Arrays For Polarimetric Optical Biosensing. Frontiers In Biological Detection: From Nanosensor To Systema Vi (2014), 89330i.
[13] J. Calderón, J. Álvarez, J. Martínez-Pastor, Polarimetric Plasmonic Sensing with Bowtie Nanoantenna Arrays, Plasmonics, 2015, 10, pp.703-711
[14] A. D. Rakić, A. B. Djurišic, J. M. Elazar, and M. L. Majewski. Optical properties of metallic films for vertical-cavity optoelectronic devices, Appl. Opt. 37 (1998) 5271-5283
[15] A. V. Kildishev, J. D. Borneman, K-P Chen, V. P. Drachev, Numerical Modeling of Plasmonic Nanoantennas with Realistic 3D Roughness and Distortion, 11, Sensors, (2011) 7178-7187